Research Article | Vol. 27, No. 18 / 2 September 2019 / Optics Express 25342
Optics EXPRESS

Spiral spectrum of a Laguerre-Gaussian beam propagating in anisotropic non-Kolmogorov turbulent atmosphere along horizontal path

JUN ZENG,[1] XIANLONG LIU,[2] CHENGLIANG ZHAO,[1,4] FEI WANG,[1,5] GREG GBUR,[3] AND YANGJIAN CAI[1,2,6]

[1] School of Physical Science and Technology, Soochow University, Suzhou 215006, China
[2] Shandong Provincial Engineering and Technical Center of Light Manipulations & Shandong Provincial Key Laboratory of Optics and Photonic Device, School of Physics and Electronics, School of Physics and Electronics, Shandong Normal University, Jinan 250014, China
[3] Department of Physics and Optical Science, University of North Carolina at Charlotte, Charlotte, North Carolina 28223, USA
[4] zhaochengliang@suda.edu.cn
[5] fwang@suda.edu.cn
[6] yangjiancai@suda.edu.cn

Abstract: Close to the ground, it is generally known that atmospheric turbulence exhibits strong anisotropy, which affects the performance of applications such as free-space optical (FSO) communication. In this paper, we establish a theoretical model for calculating the spiral spectrum, also called the orbital angular momentum (OAM) spectrum, of a Laguerre-Gaussian (LG) beam after propagation through anisotropic turbulence along a horizontal link. This model isolates the effects of anisotropy from other parameters of the turbulence. On the basis of this model, the effects of the anisotropy on the probability density of the OAM spectrum and its corresponding modal crosstalk are studied through numerical examples. Our simulation results show that the width of the OAM spectrum will increase or slightly decrease depending on the specific nature of the anisotropy. In addition, it is demonstrated that the inner scale is more likely to cause modal crosstalk than the outer scale. Some strategies to reduce modal crosstalk in anisotropic turbulence are also discussed. Our results may be useful in OAM-based FSO communication at ground level.

1. Introduction

Recently, considerable attention has been paid to vortex beams which possess orbital angular momentum (OAM), due to their potential benefits in both free-space and fiber-optical communication, in particular through the use of OAM multiplexing and modulation (encoding / decoding) [1–3]. In addition to amplitude, phase, polarization and frequency, OAM modes have been proposed as a new basis set of carrier signals allowing, in principle, an increase of the channel transmission capacity [4,5]. However, when a vortex beam propagates through the atmosphere, the wave front distortions induced by atmospheric turbulence result in mode crosstalk and increase the bit error rate, as part of the energy launched into a single OAM mode is redistributed into other modes [6]. Nevertheless, Li [7] reported that the OAM of a vortex beam disturbed by the turbulent atmosphere can be maintained using adaptive optics. The influence of turbulence on the propagation characteristics of OAM modes has been analyzed in various studies, including investigations of Laguerre-Gaussian (LG) beams [8,9], Airy beams [10], Bessel-like beams [11] and Lommel beams [12]. It has been noted, in particular, that nondiffracting beams have an advantage in free-space optical communications due to their self-healing characteristics.

#370828 https://doi.org/10.1364/OE.27.025342
Journal © 2019 Received 24 Jun 2019; revised 8 Aug 2019; accepted 9 Aug 2019; published 22 Aug 2019

Optics EXPRESS

A significant number of these studies have focused on isotropic turbulence, in which the statistical properties of the turbulence are independent of direction, and have used the venerable Kolmogorov model to describe those statistics. However, it is known that the atmosphere's statistical behavior does not always follow Kolmogorov statistics; rather, it follows a more general non-Kolmogorov spectral power law [13]. Furthermore, a variety of experimental and theoretical studies have shown that the turbulent atmosphere can also be anisotropic at ground level, in a boundary layer, or in the stratosphere [14–20]. In isotropic turbulence, the turbulent eddies – regions of uniform refractive index – are taken on average to be spherical. In anisotropic turbulence, the eddies are taken to be ellipsoids which in general can have three different semi-principal axes. In many cases, however, two semi-principal axes are the same and the third, the direction of anisotropy, is different.

Anisotropy in turbulence is pertinent to a variety of atmospheric links and meteorological conditions and can affect optical system operation. In the simplest form, the direction of anisotropy is along the direction of propagation, and this has been shown to have beneficial effects. For example, with an increase of the anisotropic coefficient, which is proportional to the atmospheric layer altitude, atmospheric turbulence has a smaller effect on an imaging system [21]. Increasing the anisotropic coefficient can effectively overcome the combined effects of beam wander and beam spreading (also known as the long-term beam spread) and reduce the scintillation index [22], as well as can improve field correlations [23] and increase temporal pulse broadening [24]. These works reveal that anisotropy plays an important role in the analysis of a beam propagating in the turbulent atmosphere.

In the aforementioned research, the anisotropy of turbulence acts only as a modifier to the turbulence's strength; this type of behavior can be seen when propagating along a vertical path [25,26]. Along horizontal paths, the anisotropic coefficients along the orthogonal axes transverse to the direction of beam propagation can be different. Andrews *et al.* [27–30] proposed a general anisotropic turbulence spectrum by introducing two anisotropic coefficients to describe the asymmetric properties of turbulent eddies along the horizontal and vertical directions. However, their model of the power spectrum intermingles the anisotropic coefficients with the refractive-index structure parameter; in particular, the term which contains the anisotropy coefficient in the numerator of the power spectrum can be regarded as a constant coefficient of the refractive-index structure parameter. With this model, a change of anisotropic coefficient can be viewed as a simultaneous variation of the refractive-index structure parameter, making it difficult to determine whether observed effects of anisotropic turbulence are caused by the anisotropy or by the strength of the turbulence.

To our knowledge, there have been no reports about the specific influence of anisotropy on the probability distribution of OAM at the receiver that distinguishes between the effects of the anisotropic coefficient and the effects of the refractive-index structure parameter. In this article, we study the effect of anisotropy on the spiral spectrum of LG beams by the use of a model which separates turbulence strength and anisotropy. This model can account for Kolmogorov and non-Kolmogorov turbulence. We introduce a rigorous formula for calculating the spiral spectrum after propagating in these general turbulence cases, and provide physical interpretations of the derived probability density and modal crosstalk, as well as guidelines for optimizing OAM detection probability.

The paper is organized as follows: in section 2, the derivation of anisotropic power spectrum at ground level is briefly reviewed; in section 3, a theoretical model for calculating the OAM spectrum of the LG beam propagation through anisotropic turbulence is derived under the Rytov approximation; in section 4, the influences of the turbulence parameters and beam parameters on the received probability density and modal crosstalk are analyzed in detail and section 5 summarizes the results.

Optics EXPRESS

2. Anisotropic power spectrum for near-ground atmospheric turbulence

In this section, we briefly review the procedure for deriving the anisotropic power spectrum of refractive-index fluctuations induced by atmospheric turbulence at ground level.

For optical wave propagation in the atmosphere, the index of refraction is one of the most important parameters affecting the propagation characteristics of optical waves. This index is very sensitive to small-scale temperature fluctuations, and these fluctuations, combined with turbulent-mixing, causes the random behavior of the refractive index in atmosphere. To visualize the development of turbulent structure, let us refer to Fig. 1(a), based on the energy cascade theory for the homogeneous and isotropic case. Large eddies, under the influence of inertial forces, break up into smaller eddies to form a continuum of eddy sizes for the transfer of energy from a macroscale L_0 (outer scale of turbulence) to a microscale l_0 (inner scale of turbulence). The eddies in this model are often assumed to be isotropic on average. However, at ground level, this isotropic behavior is broken, since the temperature of the ground is usually much higher than that of the atmosphere; this is especially true in the daytime in tropical or desert areas. As a result, the refractive index fluctuations in the vertical direction are stronger than those in directions parallel to the ground. Figure 1(b) shows the development of eddies in the anisotropic case, in which eddies become ellipsoids.

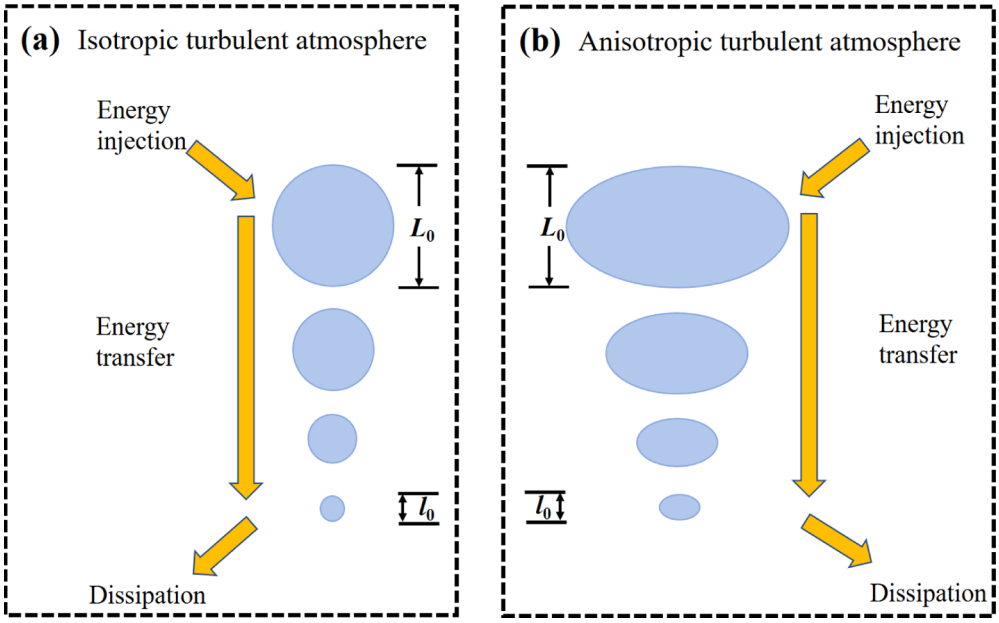

Fig. 1. Schematic for the Kolmogorov cascade theory of turbulence. (a) Isotropic atmospheric turbulence. (b) Anisotropic atmospheric turbulence. L_0 and l_0 denote the outer and inner scale of turbulence, respectively. Turbulent cells (eddies) between the scale size L_0 and l_0 form the inertial subrange. a, a', b' and c' denotes the semi-principal axes of turbulent cells in different directions, respectively.

To define the anisotropic power spectrum, let us start with a general anisotropic model for the refractive index structure function,

$$D_n(\mathbf{R}) = \beta C_n^2 \left(x^2/\mu_x^2 + y^2/\mu_y^2 + z^2/\mu_z^2\right)^{\gamma/2}, l_0 < |\mathbf{R}| < L_0, \tag{1}$$

where $\mathbf{R} = (x, y, z)$ is a spatial vector, and μ_x, μ_y, μ_z are the anisotropy coefficients along the x, y and z directions, respectively. The quantity γ is the power law of the turbulence; β is a constant

Optics EXPRESS

which is equal to unity when $\gamma = 2/3$, and otherwise has units $\mathrm{m}^{-\gamma+2/3}$. If γ is 2/3, Eq. (1) reduces to the well-known Kolmogorov model of turbulence.

According to [31], the relation between the structure function and the power spectrum in the isotropic case takes on the form

$$\Phi_n(\boldsymbol{\kappa}) = \frac{1}{4\pi^2\kappa^2}\int_0^\infty \frac{\sin(\kappa R)}{\kappa R}\frac{d}{dR}\left[R^2\frac{dD_n(\mathbf{R})}{dR}\right]dR, \tag{2}$$

where $\boldsymbol{\kappa} = (\kappa_x, \kappa_y, \kappa_z)$ is a vector spatial frequency and $\kappa = \sqrt{\kappa_x^2 + \kappa_y^2 + \kappa_z^2}$. To evaluate the anisotropic power spectrum, we make the change of variables $x = \mu_x x'$, $y = \mu_y y'$ and $z = \mu_z z'$. The resulting structure function in Eq. (1) becomes isotropic in the new spatial variable $\mathbf{R}' = (x', y', z')$. The coordinate differential dR in Eq. (2) is related to dR' by $dR = \mu_x\mu_y\mu_z dR'$, and the resulting power spectrum is isotropic in the stretched spatial frequency $\kappa' = (\kappa_x'\mu_x, \kappa_y'\mu_y, \kappa_z'\mu_z)$. After substituting Eq. (1) into Eq. (2) and integrating, we obtain the expression

$$\Phi_n(\boldsymbol{\kappa}) = \frac{\mu_x\mu_y\mu_z A(\alpha)\tilde{C}_n^2}{\left(\mu_x^2\kappa_x^2 + \mu_y^2\kappa_y^2 + \mu_z^2\kappa_z^2\right)^{\alpha/2}}, \frac{1}{l_0} < |\boldsymbol{\kappa}| < \frac{1}{L_0}, 3 < \alpha < 4, \tag{3}$$

where $\alpha = \gamma + 3$, $\tilde{C}_n^2 = \beta C_n^2$ is a generalized structure constant with units $\mathrm{m}^{3-\alpha}$, $A(\alpha)$ is a dimensionless constant, given by

$$A(\alpha) = \frac{1}{4\pi^2}\Gamma(\alpha - 1)\cos(\alpha\pi/2), \tag{4}$$

and $\Gamma(\cdot)$ in Eq. (4) is the Gamma function. However, Eq. (3) is only valid over the inertial subrange $1/l_0 < |\boldsymbol{\kappa}| < 1/L_0$. To extend the power spectrum over all spatial frequencies for mathematical convenience, we modify the power spectrum following the von Karman model widely used in treating isotropic and homogeneous turbulence,

$$\Phi_n(\boldsymbol{\kappa}, \alpha) = \frac{\mu_x\mu_y\mu_z A(\alpha)\tilde{C}_n^2 \exp\left[-\left(\mu_x^2\kappa_x^2 + \mu_y^2\kappa_y^2 + \mu_z^2\kappa_z^2\right)/\kappa_m^2\right]}{\left(\mu_x^2\kappa_x^2 + \mu_y^2\kappa_y^2 + \mu_z^2\kappa_z^2 + \kappa_0^2\right)^{\alpha/2}}, 3 < \alpha < 4, 0 < |\boldsymbol{\kappa}| < \infty, \tag{5}$$

where $\kappa_0 = 2\pi/L_0$ and $\kappa_m = c(\alpha)/l_0$, with $c(\alpha)$ being a function with α, given by

$$c(\alpha) = \left\{\frac{2\pi\Gamma\left[(5-\alpha)/2\right]A(\alpha)}{3}\right\}^{1/(\alpha-5)}. \tag{6}$$

When $\mu_x = \mu_y \neq 1$ and $\mu_z = 1$, Eq. (5) reduces to the conventional anisotropic non-Kolmogorov spectrum with circularly symmetric turbulent eddies in the $x - y$ plane stretched or compressed along the z-direction [18,27]; furthermore, when $L_0 \to \infty$ and $l_0 \to 0$, Eq. (5) reduces to the form introduced in [22]. In particular, when $\mu_x = \mu_y = \mu_z = 1$ and $\alpha = 11/3$, it reduces to the conventional isotropic Kolmogorov spectrum, i.e., $\Phi_n(\kappa_x, \kappa_y, 0) = 0.033 C_n^2 \kappa^{-11/3}$.

From Eq. (5), it is readily seen that the choice of anisotropy coefficients results in very different turbulence even for the same ratios of μ_x, μ_y, μ_z. For example, let us imagine two sets of coefficients: $(\mu_x, \mu_y, \mu_z) = (3, 1, 3)$ and $(6, 2, 6)$. They have the same ratios, but they will lead to the different results for the power spectrum, because the anisotropy coefficients are related to the other parameters in the power spectrum such as the generalized structure constant $\tilde{C}_n^2$, inner scale l_0 and outer scale L_0. In order to introduce a stronger restriction on the anisotropy coefficients, we require that the product of the coefficients satisfies the condition: $\mu_x\mu_y\mu_z = 1$. This condition implies that the eddies for isotropic turbulence and anisotropic turbulence at the

Optics EXPRESS

same altitude have the same volume, i.e., $4\pi a^3/3 = 4\pi a'b'c'/3$, where a is the average radius of eddies in the isotropic case; a', b' and c' are the average semi-principal axes of eddies in the x, y and z direction in the anisotropic case (see again Fig. 1). In the following analysis, this volume condition is always kept.

For future reference, an atmosphere with $\mu_x/\mu_y \gg 1$ has eddies resembling horizontally-extended flat circular pancakes, while an atmosphere with $\mu_x/\mu_y \ll 1$ has eddies resembling vertically-oriented needles.

3. Transmission model of the OAM mode for a LG beam propagating in anisotropic non-Kolmogorov turbulent atmosphere along horizontal path

We now consider how to simulate the propagation of a LG beam through anisotropic turbulence using the model of the previous section. A schematic of our configuration, in which a LG beam propagates at ground level through a horizontal link, is shown in Fig. 2. The y direction is vertical, and $x-z$ plane is parallel to the ground. The propagation axis of the LG beam is along the z-axis. Due to the presence of turbulence, the OAM mode spectrum at the receiver plane will be dispersed even though the OAM mode in the transmitter plane is pure. For example, if the OAM mode is of order $l = 1$ in the transmitter plane, some of the energy will leak into other neighboring modes $l = 0, 2, -1, 3\cdots$, and so forth. For simplicity, we consider a LG beam with radial order $p = 0$. In this case, the electric field of the LG beam at the receiver plane in the absence of turbulence can be written as [32,33]

$$U(r,\theta,z) = \sqrt{\frac{2}{\pi|l|!}}\frac{1}{w(z)}\left[\frac{\sqrt{2}r}{w(z)}\right]^{l}\exp\left[-\frac{r^2}{w^2(z)}\right]\exp(il\theta) \times \exp\left\{i(l+1)\tan^{-1}(z/z_R) - i\frac{kr^2}{2z\left[1+(z_R/z)^2\right]}\right\}, \tag{7}$$

where (r,θ) are the radial and azimuthal coordinates in a polar coordinate system and z is the distance between the transmitter plane and the receiver plane. Here $w(z) = w_0\sqrt{1+(z/z_R)^2}$ is the radius of the fundamental Gaussian beam at the receiver plane, w_0 is initial beam width, $z_R = kw_0^2/2$ is the Rayleigh range, and $k = 2\pi/\lambda$ is the wave number, with λ being the wavelength of the light beam. The quantity l is the topological charge, indicating the number of 2π phase cycles the beam exhibits in a counterclockwise path around the circumference of the mode.

In the presence of turbulence, the electric field of the LG beam at the receiver plane under the Rytov approximation becomes [25,29,31]

$$U_{tur}(r,\theta,z) = U(r,\theta,z)\exp[\psi(r,\theta,z)], \tag{8}$$

where $\psi(\mathbf{r},\theta,z)$ is the complex random phase perturbation induced by the turbulent atmosphere. All possible realizations of this perturbation are represented by a statistical ensemble which we will use to determine the average effects of the turbulence.

Based on the analysis in [34], we can express the $U_{tur}(r,\theta,z)$ as a superposition of spiral harmonics

$$U_{tur}(r,\theta,z) = \frac{1}{\sqrt{2\pi}}\sum_{m=-\infty}^{\infty} a_m(r,z)\exp(im\theta), \tag{9}$$

where m is an integer number, and the functions $a_m(r,z)$ are given by the integral

$$a_m(r,z) = \frac{1}{\sqrt{2\pi}}\int_0^{2\pi} U_{tur}(r,\theta,z)\exp(-im\theta)\,d\theta. \tag{10}$$

Optics EXPRESS

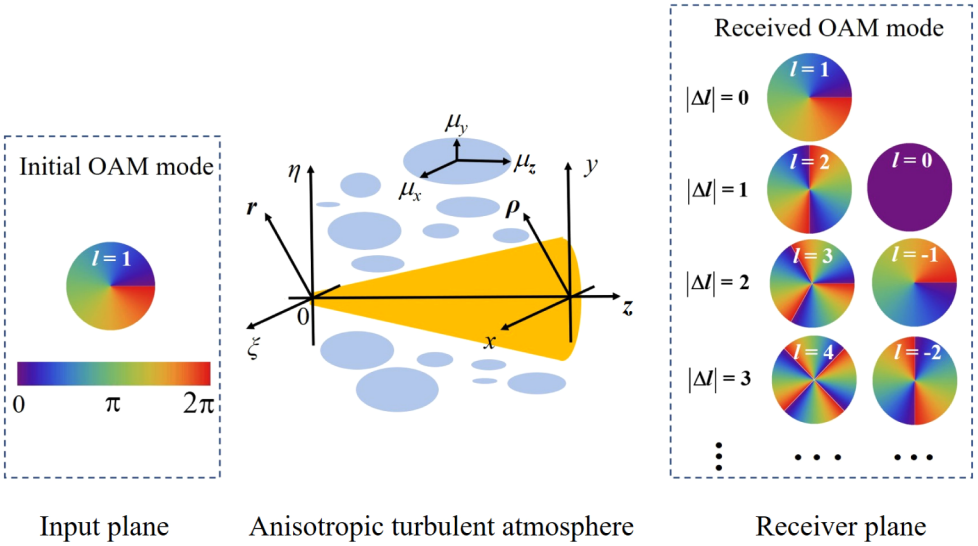

Fig. 2. Schematic diagram of the effects of an anisotropic turbulent atmosphere on the OAM mode.

The square of modulus of a_m takes the form

$$|a_m(r,z)|^2 = \frac{1}{2\pi}\int_0^{2\pi}\int_0^{2\pi} U_{tur}(r,\theta_1,z)\,U_{tur}^*(r,\theta_2,z)\exp\left[-im(\theta_1-\theta_2)\right]d\theta_1 d\theta_2. \tag{11}$$

On substituting from Eq. (7) into Eq. (11) and taking the average over the ensemble of the turbulent phase perturbations, we find that

$$\begin{aligned}\langle|a_m(r,z)|^2\rangle &= \frac{1}{2\pi}\int_0^{2\pi}\int_0^{2\pi} U(r,\theta_1,z)\,U^*(r,\theta_2,z)\exp\left[-im(\theta_1-\theta_2)\right]\\ &\times\langle\exp\left[\psi(r,\theta_1,z)+\psi^*(r,\theta_2,z)\right]\rangle d\theta_1 d\theta_2\\ &= \frac{2}{\pi|l|!}\frac{1}{2\pi}\left[\frac{1}{w(z)}\right]^2\left[\frac{\sqrt{2}r}{w(z)}\right]^{2l}\exp\left[-\frac{2r^2}{w^2(z)}\right]\\ &\times\int_0^{2\pi}\int_0^{2\pi}\exp\left[-i(m-l)(\theta_1-\theta_2)\right]\langle\exp\left[\psi(r,\theta_1,z)+\psi^*(r,\theta_2,z)\right]\rangle d\theta_1 d\theta_2,\end{aligned} \tag{12}$$

where $\langle\cdots\rangle$ stands for the ensemble average and the asterisk denotes the complex conjugate. The quantity $\langle|a_m(r,z)|^2\rangle$ represents the probability density of vortex/spiral modes in turbulence.

According to [35], the second-order statistics of the complex phase perturbation may be represented as

$$\begin{aligned}&\langle\exp\left[\psi(r,\theta_1,z)+\psi^*(r,\theta_2,z)\right]\rangle=\\ &\exp\left\{-2\pi k^2 z\int_0^1 dt\int_0^\infty d^2\boldsymbol{\kappa}_\perp\Phi_n(\boldsymbol{\kappa}_\perp,\kappa_z=0)\left[1-\exp\left(t\mathbf{r}_d\cdot\boldsymbol{\kappa}_\perp\right)\right]\right\},\end{aligned} \tag{13}$$

where $\boldsymbol{\kappa}_\perp \equiv (\kappa_x,\kappa_y)$ is the transverse spatial frequency, and $\Phi_n(\boldsymbol{\kappa})$ is the spectral power spectrum of the refractive index fluctuations shown in Eq. (5). The vector $\mathbf{r}_d \equiv \mathbf{r}_1 - \mathbf{r}_2$ is the difference between two transverse points $\mathbf{r}_1 \equiv (r,\theta_1)$ and $\mathbf{r}_2 \equiv (r,\theta_2)$. In the derivation of Eq. (13), the Markov approximation is applied, which means that the fluctuations in the refractive index are

Optics EXPRESS

delta-correlated at any pair of points along the propagation direction. To evaluate the integral, we first make the change of variable $\kappa_x = \kappa_x'/\mu_x$, $\kappa_y = \kappa_x'/\mu_y$ in Eq. (5), yielding

$$\langle \exp\left[\psi\left(r,\theta_1,z\right)+\psi^*\left(r,\theta_2,z\right)\right]\rangle = \exp\left\{-\frac{2\pi k^2 z}{\mu_x\mu_y}\int_0^1 dt\int_0^\infty d\kappa_x' d\kappa_y' \Phi_n\left(\boldsymbol{\kappa}_\perp'\right)\left[1-\exp\left(t\mathbf{r}_d'\cdot\boldsymbol{\kappa}_\perp'\right)\right]\right\}, \tag{14}$$

where $\boldsymbol{\kappa}_\perp' \equiv \left(\kappa_x', \kappa_y'\right)$, $\mathbf{r}_d' = \left(x_d/\mu_x, y_d/\mu_y\right)$. The differential $d\kappa_x' d\kappa_y'$ can be expressed in polar coordinates, i.e., $d\kappa_x' d\kappa_y' = \kappa' d\kappa' d\phi$. By then integrating over ϕ, Eq. (14) becomes

$$\langle \exp\left[\psi\left(r,\theta_1,z\right)+\psi^*\left(r,\theta_2,z\right)\right]\rangle = \exp\left\{-\frac{4\pi^2 k^2 z}{\mu_x\mu_y}\int_0^1 dt\int_0^\infty \kappa' d\kappa' \Phi_n\left(\boldsymbol{\kappa}_\perp'\right)\left[1-J_0\left(t\kappa'|\mathbf{r}_d'|\right)\right]\right\}, \tag{15}$$

where J_0 is the Bessel function of order 0.

We now restrict ourselves to the quite general case where either the points $\mathbf{r}_1$ and $\mathbf{r}_2$ are located sufficiently close to the optical axis or the inner scale of turbulence is much larger than the transverse coherence of the laser beam propagating in turbulence for a certain propagation distance [35]. Then the Bessel function can be approximated by the first two terms of its Taylor expansion, i.e., $J_0(x) = 1 - x^2/4$. By applying this condition and integrating over κ', Eq. (15) is simplified to the form

$$\langle \exp\left[\psi\left(r,\theta_1,z\right)+\psi^*\left(r,\theta_2,z\right)\right]\rangle = \exp\left(-\frac{T\mu_z x_d^2}{\mu_x^2}\right)\exp\left(-\frac{T\mu_z y_d^2}{\mu_y^2}\right), \tag{16}$$

with

$$T = \frac{\pi^2 k^2 z A(\alpha)}{6(\alpha-2)}\tilde{C}_n^2\left[\eta\kappa_m^{2-\alpha}\exp\left(\kappa_0^2/\kappa_m^2\right)\Gamma_1\left(2-\alpha/2,\kappa_0^2/\kappa_m^2\right)-2\kappa_0^{4-\alpha}\right], \tag{17}$$

$$x_d = r\left(\cos\theta_1-\cos\theta_2\right), \quad y_d = r\left(\sin\theta_1-\sin\theta_2\right), \tag{18}$$

where $\eta = 2\kappa_0^2 + (\alpha-2)\kappa_m^2$ and Γ_1 is the incomplete Gamma function. It follows from Eq. (16) that the decoherence of the light beam caused by the turbulence is strongly affected by the anisotropy coefficients μ_x, μ_y and μ_z.

Substituting from Eq. (16) into Eq. (12), we obtain the final expression of the mode probability density for spiral modes

$$\langle |a_m(r,z)|^2\rangle = \frac{1}{\pi^2|l|!}\left[\frac{1}{w(z)}\right]^2\left[\frac{\sqrt{2}r}{w(z)}\right]^{2l}\exp\left[-\frac{2r^2}{w^2(z)}\right] \times\int_0^{2\pi}\int_0^{2\pi}\exp\left[-i(m-l)(\theta_1-\theta_2)\right]\exp\left(-\frac{T\mu_z x_d^2}{\mu_x^2}\right)\exp\left(-\frac{T\mu_z y_d^2}{\mu_y^2}\right)d\theta_1 d\theta_2. \tag{19}$$

The total energy received by the detector can be written as $E = 2\varepsilon_0\sum_{m=-\infty}^{\infty} C_m$, where $C_m = \int_0^R \langle |a_m(r,z)|^2\rangle r dr$ represents the energy content for each OAM mode and R denotes the radius of the receiver aperture.

The fraction of energy possessed by the mth spiral harmonic of the transmitted LG beam is then determined by the expression,

$$P_m = C_m / \sum_{m=-\infty}^{\infty} C_q. \tag{20}$$

It is clear that a LG beam with topological charge l has the energy weight $P_m = 1$ for $m = l$ and $P_m = 0$ for $m \neq l$ at the transmitter plane, and the values of P_m remain unchanged in free-space

Optics EXPRESS

propagation (without turbulence) because the LG beams are eigenmodes of the Helmholtz equation under the paraxial approximation. When the designated OAM mode l propagates through atmospheric turbulence, the value of P_m for $m = l$ will decrease at the receiver plane due to the random phase perturbation induced by turbulence. In this case, $P_{m=l}$ can be regarded as the detection probability of the signal OAM mode l, which shows the transfer efficiency of the transmitted OAM state. For $m = l \pm \Delta l$, P_m is defined as the crosstalk probability which denotes the probability of a photon changing its OAM state, and Δl denotes the difference between the transmitted and received topological mode.

To assess the magnitude of the OAM fluctuations in turbulence, we introduce a parameter, the variance of crosstalk probability [36], defined as

$$V = \sum_{m=-\infty}^{\infty} P_m \left(m - \overline{m}\right)^2, \tag{21}$$

where $\overline{m} = \sum_{m=-\infty}^{\infty} P_m m$ denotes the average OAM at the receiver plane. It is clear that no mode crosstalk occurs when V is equal to zero. For larger V, more energy has leaked into adjacent and more distant modes.

4. Numerical results

In this section, on the basis of Eqs. (20) and (21), we numerically study the spiral spectrum (e.g., detection probability and crosstalk probability) of the received OAM modes for a LG beam propagating in an anisotropic non-Kolmogorov turbulent atmosphere along a horizontal path. At ground level, it is reasonable to assume that $\mu_x = \mu_z$, i.e. that there is no anisotropy with respect to the two horizontal axes. Recalling that we have constrained the values of the anisotropy coefficients by $\mu_x\mu_y\mu_z = 1$, the values of all three coefficients can be determined if the ratio of the μ_x to μ_y is known.

In the following numerical examples, the parameters used in the calculation are taken to be $\lambda = 1550$nm, $w_0 = 2$cm, $l = 1$, $L_0 = 1$m, $l_0 = 1$cm, $z = 2$km, $\alpha = 11/3$, $\tilde{C}_n^2 = 10^{-14}\mathrm{m}^{3-\alpha}$ and $R = 5$cm unless otherwise specified.

Figure 3 illustrates the mode crosstalk probability at the receiver plane for several different values of μ_x/μ_y. It can be seen that the mode crosstalk probability depends strongly on this ratio. As μ_x/μ_y increases, the mode crosstalk becomes more significant, implying that the received probability $l = 1$ ($\Delta l = 0$) decreases and more energy enters into other adjacent modes ($|\Delta l|>0$). Conversely, as μ_x/μ_y decreases, the mode crosstalk actually improves compared to the isotropic ($\mu_x = \mu_y$) case. We may understand these differences by looking at how the spatial coherence of the beam is affected by the anisotropy. From Eq. (16), the coherence widths of the beam in the x and y direction at the receiver plane are $\delta_x = \sqrt{\mu_x^2/\mu_z T}$ and $\delta_y = \sqrt{\mu_y^2/\mu_z T}$, respectively, defined as the $1/e$ point. Therefore, the coherence area of the beam is proportional to $\pi\delta_x\delta_y = \pi\mu_y/T$ when the condition $\mu_x = \mu_z$ is applied. One finds that the coherence area in anisotropic turbulence is only dependent on μ_y if other turbulence parameters such as the generalized structure constant, inner scale and outer scale are fixed. As the value of μ_x/μ_y increases, μ_y decreases, which means that the spatial coherence of the beam decreases. The increase in mode crosstalk probability can be therefore explained by the scrambling of the phase of the beam by the anisotropic turbulence. As μ_x/μ_y decreases, μ_y increases, which implies that the spatial coherence of the beam is larger, and less scrambled by the atmosphere.

Figure 4(a) shows the variation of the detection probability $P_{m=l}$ ($\Delta l = 0$) with μ_x/μ_y and Fig. 4(b) shows the variance of crosstalk probability V with μ_x/μ_y for different values of initial topological charge l. As expected, $P_{m=l}$ decreases as μ_x/μ_y increases, irrespective of the initial l, and the corresponding V becomes large. However, a beam with larger l experiences more significant crosstalk than one with smaller l, leading to small $P_{m=l}$ and large V at fixed μ_x/μ_y. It

Optics EXPRESS

is reasonable to believe that this higher crosstalk arises because the higher-order vortex modes have a more rapidly-varying phase, making them more susceptible to turbulence-induced phase distortion. Furthermore, higher-order vortex modes have a larger radius on propagation, leaving them exposed to a larger cross-section of the turbulence.

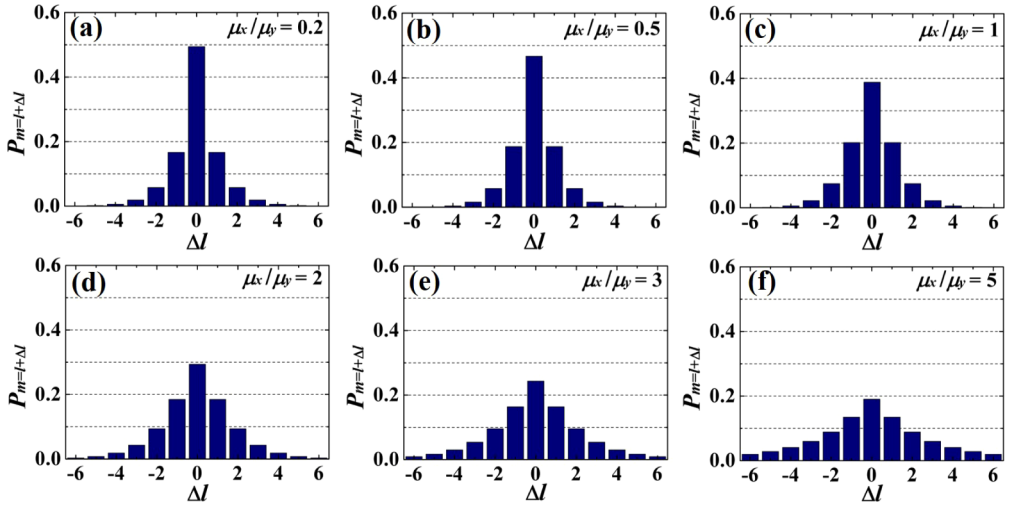

Fig. 3. Different order crosstalk probability of a LG beam with $l = 1$ propagating in anisotropic turbulent atmosphere for different values of μ_x/μ_y.

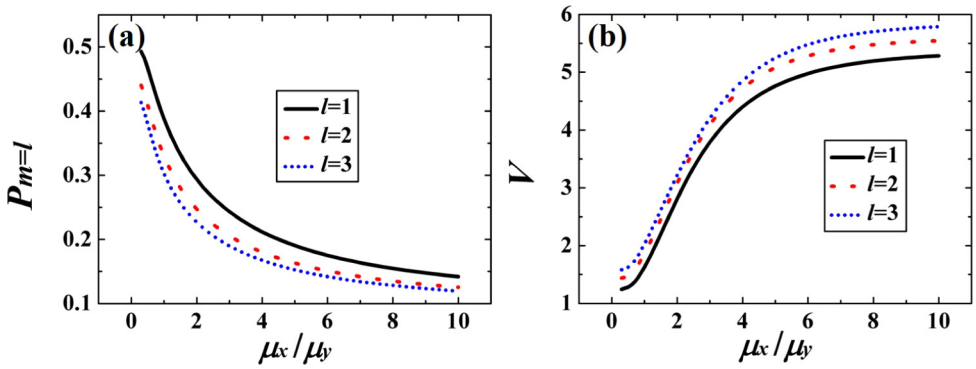

Fig. 4. Detection probability $P_{m=l}$ and the dimensionless variance of crosstalk probability V of a LG beam as a function of μ_x/μ_y for different values of l.

Figures 5(a) and 5(b) show the variation of $P_{m=l}$ and V as a function of propagation distance z for three different values of μ_x/μ_y, respectively. As expected, one can see that the value of $P_{m=l}$ decreases and the corresponding V increases as the distance z increases, regardless of μ_x/μ_y, as the effects of turbulence inevitably accumulate.

To investigate the behavior of the crosstalk probability with different orders $P_{m=l+\Delta l}$ ($\Delta l \neq 0$), we plot in Figs. 5(c) and 5(d) the variance of $P_{m=l+\Delta l}$ (e.g., $\Delta l = 1, 2, 3, 4$) with propagation distance. For simplicity, we only plot the crosstalk probability for Δl>0; the extension to the case for Δl<0 is straightforward since $P_{m=l-\Delta l} = P_{m=l+\Delta l}$. In Fig. 5(d), the main crosstalk probability $P_{m=l+\Delta l}$ ($\Delta l = 1$) first increases rapidly, reaches a maximum value, and then appears to decrease as the propagation distance z increases. As the beam begins to propagate, the turbulence scatters

Optics EXPRESS

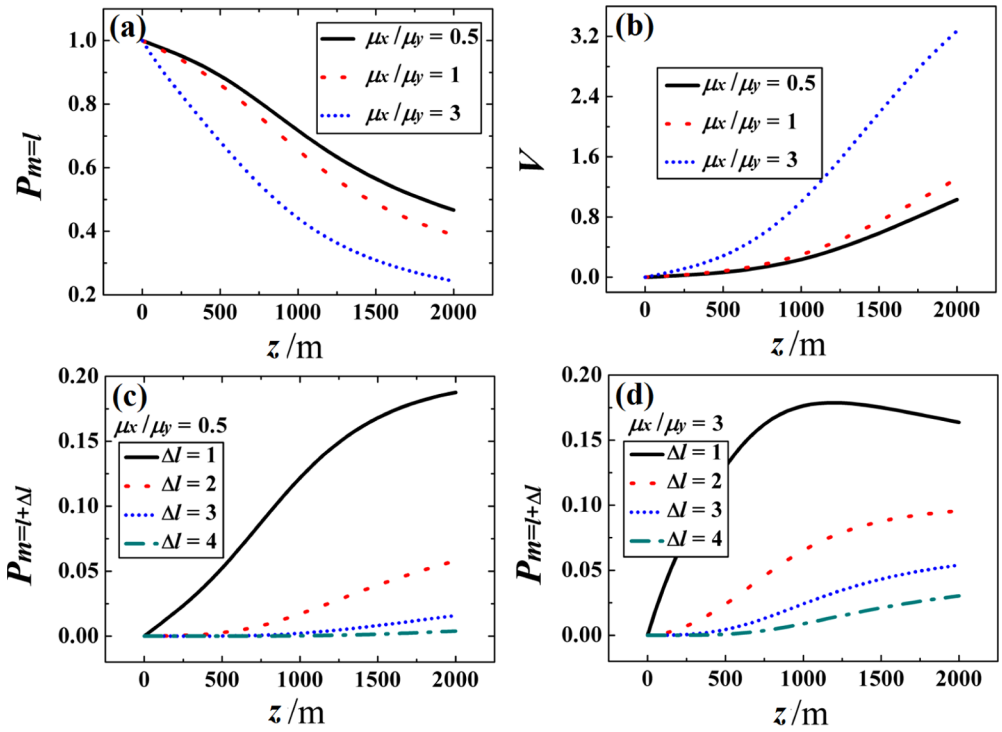

Fig. 5. (a) Detection probability $P_{m=l}$, (b) the variance of crosstalk probability V, (c-d) different order crosstalk probability $P_{m=l+\Delta l}$ of a LG beam as a function of propagation distance for several cases of anisotropy.

energy exclusively into the $\Delta l = 1$ mode, causing a rapid increase; as it propagates further, energy continues to scatter to more distant modes, causing a decline, but also can scatter back into the $\Delta l = 1$ mode, making the reduction of $P_{m=l+1}$ slower than its increase.

We now investigate the influence of the other turbulence parameters, such as power law index α, inner scale l_0 and outer scale L_0, on the detection probability $P_{m=l}$. Figure 6(a) presents the changes of $P_{m=l}$ with the power law index for different inner scales l_0.

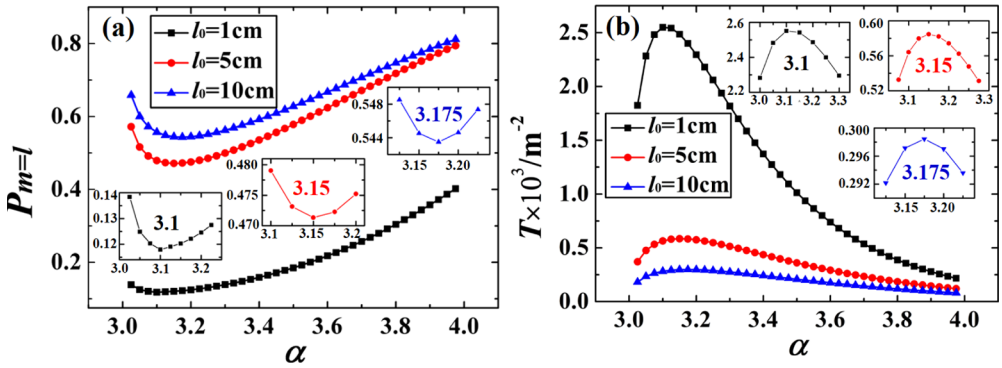

Fig. 6. (a) Detection probability and (b) T of a LG beam plotted as a function of α for several inner scales of turbulence l_0 with $\mu_x/\mu_y = 3$.

Optics EXPRESS

The anisotropy ratio in the calculation is set as $\mu_x/\mu_y = 3$. $P_{m=l}$ first decreases as α increases, reaches a minimum value when α is about 3.1, and then increases with further increase of α. Such phenomenon indicates that the LG beam suffers the most serious perturbation when α is about 3.1. According to Eq. (16), it is shown that this variation is closely related to the parameter T. In Fig. 6(b), the variation of T against the power law index is plotted. The value of T is proportional to the strength of turbulence, namely, the larger T is, the stronger the turbulence is. Therefore, the maximum value of T corresponds to the minimum value of $P_{m=l}$. In addition, one finds that the value of α will drift slightly with the change of l_0 when $T/P_{m=l}$ reaches maxima/minima. For example, for l_0 =1cm, 5cm and 10cm, the values of α are 3.1, 3.15 and 3.175, respectively [see the inset figures in Figs. 6(a) and 6(b)].

Figure 7(a) shows the dependence of the detection probability $P_{m=l}$ on the inner scale l_0 and the outer scale L_0. Relative to L_0, l_0 plays a much greater role in determining the detection probability. When the outer scale is larger than 4m, it has almost no effect on the detection probability. It is known that the main effect of the outer scale on the beam is to cause the beam position to randomly drift (also called beam wander), while the inner scale gives rise to intensity fluctuations (scintillation) in the beam, or can even cause the beam to split into several pieces, destroying the original LG mode. Thus, the detection probability dramatically drops as the inner scale decreases. Beam wander, conversely, can cause the beam to miss the detector, but maintains the vortex structure on propagation. The dependence of the generalized structure constant and the wavelength of light on the detection probability is illustrated in Fig. 7(b). The detection probability decreases with the increase of structure constant $\tilde{C}_n^2$ or with the decrease of wavelength λ. As expected, a beam with long wavelength is more suitable for OAM communications owing to it being less susceptible to the turbulent atmosphere.

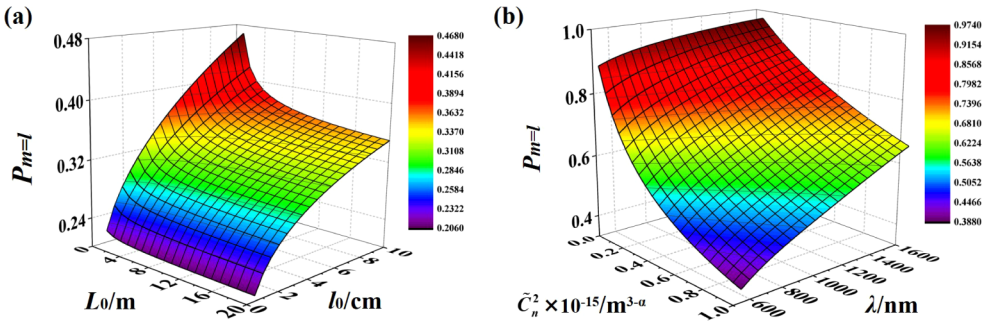

Fig. 7. Detection probability of a LG beam propagating in anisotropic turbulent atmosphere for different values of the inner scales of turbulence, outer scales of turbulence, refractive-index structure parameters and beam wavelengths. The anisotropy parameter is chosen to be $\mu_x/\mu_y = 3$.

Finally, let us investigate the effects of the initial beam width w_0 and the radius of receiver aperture R on the detection probability in anisotropic turbulence. Figure 8(a) displays detection probability $P_{m=l}$ as a function of the beam width w_0, and it can be seen that there exists an optimum value of w_0 (represented as w_{0m}) for any given z where $P_{m=l}$ reaches a maximum value. This optimal w_{0m} increases as the propagation distance increases. The calculated w_{0m} are about 2.2cm, 2.7cm and 3.1cm for z = 1km, 1.5km and 2km, respectively.

Quite remarkably, this optimal value is approximately the same for different values of anisotropy, turbulence strength, and detector size. This was tested for anisotropy ranging from $\mu_x/\mu_y = 0.5$ to $\mu_x/\mu_y = 3$, for turbulence strength ranging from $\tilde{C}_n^2 = 10^{-15}$ m$^{3-\alpha}$ to $\tilde{C}_n^2 = 10^{-14}$ m$^{3-\alpha}$, and for different aperture sizes ranging from 2cm to 6cm. In all cases, the optimal value was the same for each propagation distance, though the maximum value of $P_{m=l}$ changes.

Optics EXPRESS

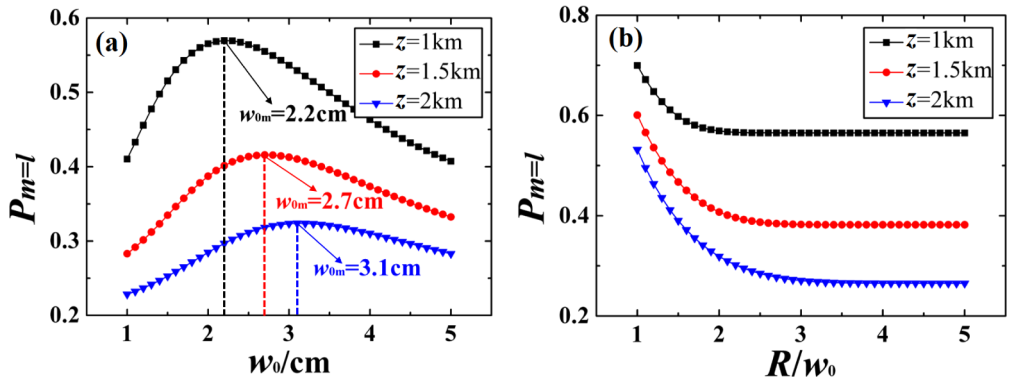

Fig. 8. Detection probability of a LG beam propagating in anisotropic turbulence atmosphere along horizontal path as a function of propagation distance for different values of the beam width w_0 and the radius of the receiver aperture R with w_0=2cm.

The value of this optimal width apparently satisfies a very simple mathematical formula. Let us recall that the radius of a LG beam intensity ring on free-space propagation, measured from the beam center to a radial point of maximum intensity, is given by [37,38],

$$r(z) = w_0\,(l/2)^{1/2}\sqrt{1+(z/z_R)^2}, \tag{22}$$

where z_R is the Rayleigh range. Table 1 presents $r(z)$ as a function of w_0 for several propagation distances, with $l = 1$. It is important to note that $r(z)$ is smaller than the Gaussian width $w(z)$ of Eq. (7), due to the presence of $\sqrt{2}$ in the denominator. It is seen that the optimal detection probability shown in Fig. 8(a) occurs when w_0 is chosen to have the minimum value $r(z)$ (marked with red). Since $r(z)$ can be calculated analytically, we have found a very easy way to determine the beam width that optimizes the detection probability.

Table 1. Radius of a LG Beam Spot against Initial Beam Width for Several Propagation Distances

	z = 1km	z = 1.5km	z = 2km
w_0/cm	$r(z)$/cm	$r(z)$/cm	$r(z)$/cm
2.0	2.246	2.974	3.764
2.1	2.228	2.901	3.63
2.2	**2.221**	2.842	3.533
2.3	2.224	2.797	3.442
2.4	2.235	2.763	3.366
2.5	2.252	2.740	3.304
2.6	2.276	2.726	3.253
2.7	2.305	**2.721**	3.213
2.8	2.339	2.723	3.183
2.9	2.377	2.732	3.161
3.0	2.419	2.746	3.148
3.1	2.464	2.767	**3.141**
3.2	2.512	2.792	3.142
3.3	2.562	2.821	3.149

Optics EXPRESS

The origin of this result is hinted at in Eq. (19), and the small values of T in Fig. 6(b). The integral over θ_1 and θ_2 depends on the turbulence only through the slowly-varying exponents in Eq. (19), which will be approximately constant and independent of the turbulence strength. Though the distribution of OAM at the detector depends in a complicated way upon the turbulence structure, evidently the optimal beam size is dominated by the propagation characteristics of the beam in free space. We note that our results are restricted to weak turbulence, and that this optimal size will likely change in strong turbulence.

In Fig. 8(b), it can be seen that $P_{m=l}$ first decreases and then tends to a saturation value as R is increased. Moreover, the larger z is, the larger the R is required for reaching the stable value. According to Eqs. (19) and (20), the mode weight for each C_m [the numerator of Eq. (20)] increases with the increase of R, but the denominator of Eq. (20) increases faster than the numerator of Eq. (20). Thus, an increment of R leads to the detection probability decreases. When the R is sufficiently large, i.e., the whole beam spot is included in the receiver aperture, the detection probability is no longer dependent on R.

5. Summary

Anisotropy in turbulence has received considerable attention in recent years and can significantly affect the performance of important optical systems such as free-space optical communications and LIDAR. An understanding of how the OAM spectrum of a LG beam evolves in such a media is hence necessary, in order to optimally increase the data transmission rate based on OAM multiplexing technology.

Here we have developed a theoretical model for calculating the spiral/OAM spectrum of LG beam propagation through anisotropic turbulence at ground level. On the basis of the derived model, the specific influence of turbulence parameters such as the anisotropy coefficient, power law index, outer scale and inner scale on the OAM detection probability have been investigated in detail through some numerical examples. In addition, the effects of the initial beam width and wavelength on detection probability are also presented. Our results reveal that the detection probability decreases monotonically as the ratio of the anisotropy coefficient in the x direction to that in the y direction, i.e., μ_x/μ_y, increases, which means anisotropy in turbulence generally plays a negative role in OAM based communication. However, there exists an optimum initial beam width for enhancing the detection probability, which can reduce the effects of anisotropy to some extent. Further, utilizing a long wavelength for a transmitted beam is also applicable to improve the detection probability. Our findings may be helpful in the design of an OAM-based free-space optical communications link in anisotropic turbulence.

Funding

National Natural Science Foundation of China (11525418, 11774250, 11804198, 11874046, 91750201); Priority Academic Program Development of Jiangsu Higher Education Institutions; Qinglan Project of Jiangsu Province of China.

References

1. Y. Ren, Z. Wang, P. Liao, L. Li, G. Xie, H. Huang, Z. Zhao, Y. Yan, N. Ahmed, A. Willner, M. P. J. Lavery, N. Ashrafi, S. Ashrafi, R. Bock, M. Tur, I. B. Djordjevic, M. A. Neifeld, and A. E. Willner, "Experimental characterization of a 400 Gbit/s orbital angular momentum multiplexed free-space optical link over 120 m," Opt. Lett. **41**(3), 622–625 (2016).
2. A. E. Willner, Y. Ren, G. Xie, Y. Yan, L. Li, Z. Zhao, J. Wang, M. Tur, A. F. Molisch, and S. Ashrafi, "Recent advances in high-capacity free-space optical and radio-frequency communications using orbital angular momentum multiplexing," Philos. Trans. R. Soc., A **375**(2087), 20150439 (2017).
3. A. Wang, L. Zhu, L. Wang, J. Ai, S. Chen, and J. Wang, "Directly using 8.8-km conventional multi-mode fiber for 6-mode orbital angular momentum multiplexing transmission," Opt. Express **26**(8), 10038–10047 (2018).
4. A. Trichili, A. B. Salem, A. Dudley, M. Zghal, and A. Forbes, "Encoding information using Laguerre Gaussian modes over free space turbulence media," Opt. Lett. **41**(13), 3086–3089 (2016).

Optics EXPRESS

5. L. Zhu, J. Liu, Q. Mo, C. Du, and J. Wang, "Encoding/decoding using superpositions of spatial modes for image transfer in km-scale few-mode fiber," Opt. Express **24**(15), 16934–16944 (2016).
6. J. A. Anguita, M. A. Neifeld, and B. V. Vasic, "Turbulence-induced channel crosstalk in an orbital angular momentum-multiplexed free-space optical link," Appl. Opt. **47**(13), 2414–2429 (2008).
7. N. Li, X. Chu, P. Zhang, X. Feng, C. Fan, and C. Qiao, "Compensation for the orbital angular momentum of a vortex beam in turbulent atmosphere by adaptive optics," Opt. Laser Technol. **98**, 7–11 (2018).
8. Y. Yuan, D. Liu, Z. Zhou, H. Xu, J. Qu, and Y. Cai, "Optimization of the probability of orbital angular momentum for Laguerre-Gaussian beam in Kolmogorov and non-Kolmogorov turbulence," Opt. Express **26**(17), 21861–21871 (2018).
9. Y. Jiang, S. Wang, J. Zhang, J. Qu, and H. Tang, "Spiral spectrum of Laguerre-Gaussian beam propagation in non-Kolmogorov turbulence," Opt. Commun. **303**, 38–41 (2013).
10. P. Li, S. Liu, T. Peng, X. Gan, and J. Zhao, "Spiral autofocusing Airy beams carrying power-exponent-phase vortices," Opt. Express **22**(7), 7598–7606 (2014).
11. Y. Zhu, X. Liu, J. Gao, Y. Zhang, and F. Zhao, "Probability density of the orbital angular momentum mode of Hankel-Bessel beams in an atmospheric turbulence," Opt. Express **22**(7), 7765–7772 (2014).
12. L. Yu, B. Hu, and Y. Zhang, "Intensity of vortex modes carried by Lommel beam in weak-to-strong non-Kolmogorov turbulence," Opt. Express **25**(16), 19538–19547 (2017).
13. I. Toselli, L. C. Andrews, R. L. Phillips, and V. Ferrero, "Free space optical system performance for laser beam propagation through non-Kolmogorov turbulence," Opt. Eng. **47**(2), 026003 (2008).
14. A. Consortini, L. Ronchi, and L. Stefanutti, "Investigation of Atmospheric Turbulence by Narrow Laser Beams," Appl. Opt. **9**(11), 2543–2547 (1970).
15. R. Manning, "An anisotropic turbulence model for wave propagation near the surface of the Earth," IRE Trans. Antennas Propag. **34**(2), 258–261 (1986).
16. M. S. Belen'Kii, S. J. Karis, C. L. Osmon, J. M. Brownn II, and R. Q. Fugate, "Experimental evidence of the effects of non-Kolmogorov turbulence and anisotropy of turbulence," Proc. SPIE **3749**, 50–51 (1999).
17. L. Biferale and I. Procaccia, "Anisotropy in turbulent flows and in turbulent transport," Phys. Rep. **414**(2-3), 43–164 (2005).
18. L. C. Andrews, R. L. Phillips, R. Crabbs, and T. Leclerc, "Deep turbulence propagation of a Gaussian-beam wave in anisotropic non-Kolmogorov turbulence," Proc. SPIE **8874**, 887402 (2013).
19. I. Toselli, "Introducing the concept of anisotropy at different scales for modeling optical turbulence," J. Opt. Soc. Am. A **31**(8), 1868–1875 (2014).
20. C. Robert, J. M. Conan, V. Michau, J. B. Renard, C. Robert, and F. Dalaudier, "Retrieving parameters of the anisotropic refractive index fluctuations spectrum in the stratosphere from balloon-borne observations of stellar scintillation," J. Opt. Soc. Am. A **25**(2), 379–393 (2008).
21. L. Cui, B. Xue, X. Cao, and F. Zhou, "Atmospheric turbulence MTF for optical waves' propagation through anisotropic non-Kolmogorov atmospheric turbulence," Opt. Laser Technol. **63**, 70–75 (2014).
22. I. Toselli, B. Agrawal, and S. Restaino, "Light propagation through anisotropic turbulence," J. Opt. Soc. Am. A **28**(3), 483–488 (2011).
23. Y. Ata and Y. Baykal, "Field correlation of flat-topped beams in anisotropic non-Kolmogorov turbulent atmosphere," J. Mod. Opt. **66**(2), 130–135 (2019).
24. C. Chen, H. Yang, S. Tong, B. Ren, and Y. Li, "Characterization of temporal pulse broadening for horizontal propagation in strong anisotropic atmospheric turbulence," Opt. Express **23**(4), 4814–4828 (2015).
25. Y. Li, L. Yu, and Y. Zhang, "Influence of anisotropic turbulence on the orbital angular momentum modes of Hermite-Gaussian vortex beam in the ocean," Opt. Express **25**(11), 12203–12215 (2017).
26. L. Cui, "Analysis of angle of arrival fluctuations for optical waves propagation through weak anisotropic non-Kolmogorov turbulence," Opt. Express **23**(5), 6313–6325 (2015).
27. L. C. Andrews, R. L. Phillips, and R. Crabbsa, "Propagation of a Gaussian-beam wave in general anisotropic turbulence," Proc. SPIE **9224**, 922402 (2014).
28. I. Toselli and O. Korotkova, "General scale-dependent anisotropic turbulence and its impact on free space optical communication system performance," J. Opt. Soc. Am. A **32**(6), 1017–1025 (2015).
29. M. Cheng, L. Guo, J. Li, and Q. Huang, "Propagation properties of an optical vortex carried by a Bessel-Gaussian beam in anisotropic turbulence," J. Opt. Soc. Am. A **33**(8), 1442–1450 (2016).
30. X. Yan, L. Guo, M. Cheng, J. Li, Q. Huang, and R. Sun, "Probability density of orbital angular momentum mode of autofocusing Airy beam carrying power-exponent-phase vortex through weak anisotropic atmosphere turbulence," Opt. Express **25**(13), 15286–15298 (2017).
31. L. C. Andrews and R. L. Phillips, *Laser Beam Propagation through Random Media* (SPIE, 2005).
32. L. Allen, M. W. Beijersbergen, R. J. C. Spreeuw, and J. P. Woerdman, "Orbital angular momentum of light and the transformation of Laguerre-Gaussian laser modes," Phys. Rev. A **45**(11), 8185–8189 (1992).
33. M. W. Beijersbergen, L. Allen, H.E. L. O. Van Der Veen, and J. P. Woerdman, "Astigmatic laser mode converters and transfer of orbital angular momentum," Opt. Commun. **96**(1-3), 123–132 (1993).
34. L. Torner, J. P. Torres, and S. Carrasco, "Digital spiral imaging," Opt. Express **13**(3), 873–881 (2005).
35. H. T. Yura, "Mutual Coherence Function of a Finite Cross Section Optical Beam Propagating in a Turbulent Medium," Appl. Opt. **11**(6), 1399–1406 (1972).

Optics EXPRESS

36. R. Zambrini and S. M. Barnett, "Quasi-Intrinsic Angular Momentum and the Measurement of Its Spectrum," Phys. Rev. Lett. **96**(11), 113901 (2006).
37. V. P. Lukin, P. A. Konyaev, and V. A. Sennikov, "Beam spreading of vortex beams propagating in turbulent atmosphere," Appl. Opt. **51**(10), C84–C87 (2012).
38. X. Ge, B. Wang, and C. Guo, "Evolution of phase singularities of vortex beams propagating in atmospheric turbulence," J. Opt. Soc. Am. A **32**(5), 837–842 (2015).